2005

A Proper Approach for Nonequilibrium Molecular Dynamics Simulations of Planar Elongational Flow

David J. Keffer
University of Tennessee - Knoxville

C. Baig
University of Tennessee - Knoxville

B. J. Edwards
University of Tennessee - Knoxville

H. D. Cochran
University of Tennessee - Knoxville

Recommended Citation
C. Baig, B. J. Edwards, D. J. Keffer, and H. D. Cochran, J. (2005). A proper approach for nonequilibrium molecular dynamics simulations of planar elongational flow. Chem. Phys. 122, 114103 DOI:10.1063/1.1819869

A proper approach for nonequilibrium molecular dynamics simulations of planar elongational flow

C. Baig, B. J. Edwards, and D. J. Keffer
Department of Chemical Engineering, University of Tennessee, Knoxville, Tennessee 37996-2200

H. D. Cochran[a)]
Department of Chemical Engineering, University of Tennessee, Knoxville, Tennessee 37996-2200 and Chemical Sciences Division, Oak Ridge National Laboratory, Oak Ridge, Tennessee 37831-6181

(Received 27 February 2004; accepted 27 September 2004; published online 17 March 2005)

We present nonequilibrium molecular dynamics simulations of planar elongational flow (PEF) by an algorithm proposed by Tuckerman *et al.* [J. Chem. Phys. **106**, 5615 (1997)] and theoretically elaborated by Edwards and Dressler [J. Non-Newtonian, Fluid Mech. **96**, 163 (2001)], which we shall call the proper-SLLOD algorithm, or *p*-SLLOD for short. [For background on names of algorithms see W. G. Hoover, D. J. Evans, R. B. Hickman, A. J. C. Ladd, W. T. Ashurst, and B. Moran, Phys. Rev. A **22**, 1690 (1980) and D. J. Evans and G. P. Morriss, Phys. Rev. A **30**, 1528 (1984).] We show that there are two sources for the exponential growth in PEF of the total linear momentum of the system in the contracting direction, which has been previously observed using the so-called SLLOD algorithm. The first comes from the SLLOD algorithm itself, and the second from the implementation of the Kraynik and Reinelt [Int. J. Multiphase Flow **18**, 1045 (1992)] boundary conditions. Using the *p*-SLLOD algorithm (to eliminate the first source) implemented with our simulation strategy (to eliminate the second) in PEF simulations, we no longer observe the exponential growth. By analyzing the equations of motion, we also demonstrate that both the SLLOD and the DOLLS algorithms are intrinsically unsuitable for representing a nonequilibrium system with elongational flow. However, the *p*-SLLOD algorithm has a rigorously canonical structure in laboratory phase space, and thus can represent a nonequilibrium system not only for elongational flow but also for a general flow. © *2005 American Institute of Physics.*
[DOI: 10.1063/1.1819869]

I. INTRODUCTION

Understanding the flow behavior of complex fluids remains a problem of great fundamental and practical significance. The understanding of homogeneous shear flow has been substantially advanced by the combined results of experiments, theory, and nonequilibrium molecular dynamics (NEMD) simulations. However, understanding of elongational flows and more general flows, which are also of fundamental and practical importance, has been frustrated by the absence of a suitable NEMD algorithm for steady-state flows other than shear flow. It is our purpose in this work to demonstrate a theoretically sound algorithm for steady-state planar elongational flow (PEF) and to elucidate the deficiencies in recent attempts toward this end. With a sound algorithm for NEMD of PEF, rigorous testing of theories of PEF are made possible, and predictions of complex fluids undergoing extensional flow, such as in polymer processing, may be undertaken.

There exist two well-known algorithms for simulating a nonequilibrium physical system under a specified external flow field, e.g., simple shear flow [see Eq. (17)], the so-called DOLLS tensor algorithm developed by Hoover *et al.*[1] and the SLLOD algorithm of Evans and Morriss.[2] It has been proven that, although the DOLLS algorithm has a Hamiltonian and canonical equations of motion, it makes an incorrect prediction for shear flow at high values of shear rate.[2,3] In contrast, even though the SLLOD algorithm does not have a Hamiltonian and canonical equations of motion, it predicts correctly the nonequilibrium behavior of physical systems under shear. Accordingly, extensive use has been made of the SLLOD algorithm in simulating sheared fluids.

Another practically important class of flow fields is elongational flows [see Eq. (17)], such as uniaxial, biaxial, and (the focus of this work) planar elongational flows. The main difficulty of simulating elongational flows lies in the limited simulation time available due to the contraction of one or two dimensions.[4] This problem, however, has been partially resolved by Kraynik and Reinelt's[5] ingenious discovery of the temporal and spatial periodicity of lattice vectors in PEF. Unfortunately, these authors proved that no such periodicity exists for uniaxial or biaxial elongational flow. Employing their idea, there have been several NEMD simulations of PEF using the SLLOD algorithm.[4–7]

Very recently, however, Todd and Daivis[8] have observed another serious problem in *N*-*V*-*T* NEMD simulations of PEF when using the SLLOD algorithm: the exponential growth of the total linear momentum in the contracting direction, which results in an aphysical phase transition after a certain time interval. The phenomenon starts from a nonzero

a)Author to whom correspondence should be addressed. Electronic mail: hdc@ornl.gov

initial total linear momentum of the system due to the limit of numerical precision (truncation error) in computer simulations.[8] Accepting this source as numerically unavoidable, the underlying cause is ascribed to the basic algorithm used in the simulations. As shown by Todd and Daivis, the exponential growth of the total linear momentum does not depend on the thermostat (Nosé-Hoover or Gaussian), the size of the time step (small or large), the dimensionality of the fluids (2- or 3-dimensional), or the integration scheme (Gear predictor-corrector or velocity Verlet). They showed analytically that the true cause arises intrinsically from the SLLOD algorithm itself. Although they proposed two *ad hoc* ways to avoid the problem by rescaling particle momenta at each time step or by introducing another constraint into the momentum equation, those methods disturb the natural evolution of the physical system and thus still seem undesirable. Therefore, one cannot simulate elongational flows appropriately using the SLLOD algorithm.

This situation has led us to seek another NEMD algorithm for simulating PEF, as shown below. It is not restricted to PEF but is valid for a general flow field. With remarkable insight, Tuckerman *et al.*[9] proposed a new algorithm for NEMD simulations, which they called the generalized-SLLOD algorithm. They pointed out that, whereas the SLLOD algorithm does not satisfy Newton's equations of motion, $m_i d^2\mathbf{q}_i/dt^2=\mathbf{F}_i$, the new algorithm does so. There is also a conserved quantity associated with this algorithm—see below. This algorithm was later derived by Edwards and Dressler[10] through a fundamental investigation of the canonical structure of the evolution equations under the Poisson bracket formalism. This derivation demonstrated the redundancy of the additional variable introduced by Tuckerman *et al.*[9] and illustrated the connection between the laboratory and convecting coordinates systems in NEMD algorithms. Here, we propose to call the new algorithm the ''proper-SLLOD algorithm,'' or p-SLLOD, in order to emphasize the fundamental properties of this algorithm for arbitrary flow fields.

We show in this paper that there are, in fact, two sources for the unphysical exponential growth of the total linear momentum in PEF simulations with the SLLOD algorithm. The first comes from the SLLOD algorithm itself, and the second, from the implementation of the Kraynik and Reinelt boundary conditions (KRBCs). Employing the p-SLLOD algorithm (which removes the first source [compare Eqs. (38) and (39)] in NEMD simulations), together with an appropriate simulation implementation (which removes the second source [described in Sec. IV]), we have found that we no longer face the aphysical phenomenon encountered by Todd and Daivis in NEMD simulations of PEF.

Because this work is somewhat lengthy and difficult, we take extra pains to help guide the reader through the logic of our analysis. In Sec. II, we present a theoretical analysis of all three NEMD algorithms (DOLLS, SLLOD, and p-SLLOD) in order to clarify why the p-SLLOD algorithm, rather than the DOLLS or the SLLOD algorithms, is our preferred algorithm and can be used in NEMD simulations for any flow field. Our analysis of the NEMD algorithms starts with a study of the transformation between peculiar and laboratory phase spaces $(\mathbf{p},\mathbf{q})$ and $(\mathbf{p}',\mathbf{q}')$, respectively, (see Sec. II for their definitions) and leads to conclusions regarding whether or not each algorithm has a Hamiltonian and obeys Newton's equations of motion for both shear flows and PEF. Section III compares the evolution equations of the total linear momentum (the problematic issue identified by Todd and Daivis[8]) of the three algorithms for both simple shear flow and PEF. It is shown that the SLLOD and p-SLLOD algorithm are identical for simple shear flow, but that the SLLOD algorithm for PEF omits a necessary term. Then, in Sec. IV, we detail the simulation strategy used in the present work. The results of the NEMD simulations are presented in Sec. V, where we discuss the results using the p-SLLOD and the SLLOD algorithms, including a direct comparison. We note that, because the SLLOD algorithm for PEF omits a necessary term, the results differ from those given by the p-SLLOD algorithm, especially at high strain rates. This can be vitally important in testing theories of PEF with model fluids for which NEMD of PEF can now be considered essentially exact. In addition, our results demonstrate that there are two causes for the artificial exponential growth of the momentum and the resulting phase change, which have been observed with SLLOD simulations of PEF. Both have been successfully addressed with the approach presented here. Finally, we make brief concluding remarks in Sec. VI.

The main body of this paper deals primarily with the consistency of NEMD algorithms with principles of Hamiltonian and Newtonian mechanics. In two appendices, we examine the consistency of the algorithms from the perspective of macroscopic thermodynamics. The two appendices offer derivations of the time derivative of the internal energy and discuss its implications on the pressure tensor.

II. ANALYSIS OF NEMD ALGORITHMS

In this section we analyze the three NEMD algorithms by examining them in both ''peculiar'' and ''laboratory'' frames of reference, which may be used to describe a nonequilibrium physical system under a specified external velocity field. This analysis allows us later to elucidate the basis for differences among the three algorithms. Thus, there are two kinds of momenta, the so-called ''peculiar momenta'' $\mathbf{p}$ and ''laboratory momenta'' $\mathbf{p}'$.[3] The former are defined as particle momenta with respect to a reference frame moving with the streaming velocity $\mathbf{u}$ of a fluid element containing the particles, and the latter with respect to a spatially fixed reference frame. The fluid element in the definition of the peculiar momenta is thermodynamic, in that it contains a very large number of particles, but is still infinitesimal with respect to the macroscopic world of the hydrodynamic equations. We may choose either of the two different sets of phase-space variables $(\mathbf{p},\mathbf{q})$ or $(\mathbf{p}',\mathbf{q}')$ for representing nonequilibrium systems. Denoting an imposed external velocity gradient field by $\nabla\mathbf{u}$, the two sets are related to each other by[10]

$$\begin{aligned}\mathbf{p}_i' &= \mathbf{p}_i + m_i\mathbf{q}_i\cdot\nabla\mathbf{u},\\ \mathbf{q}_i' &= \mathbf{q}_i,\end{aligned} \tag{1}$$

where m_i and $\mathbf{q}_i$ are, respectively, the mass and position vector of particle i.

In order to understand the fundamental structure of a NEMD algorithm fully, it is essential first to investigate the phase space on which it is built. In general, there exist two independent methods of canonical transformation between phase spaces: the generating function approach and the symplectic approach.[11] Here we use the symplectic approach. From the well-known property that the Poisson bracket remains unchanged under a canonical transformation,[11] it follows that the necessary and sufficient condition for a canonical transformation is

$$\mathbf{MAM}^T = \mathbf{A}, \tag{2}$$

where $\mathbf{M}^T$ is the transpose of matrix $\mathbf{M}$. For a system with s degrees of freedom, the matrices $\mathbf{M}$ and $\mathbf{A}$ are defined as

$$\mathbf{M} = \begin{bmatrix} \frac{\partial q_1'}{\partial q_1} & \cdots & \frac{\partial q_1'}{\partial q_s} & \frac{\partial q_1'}{\partial p_1} & \cdots & \frac{\partial q_1'}{\partial p_s} \\ \vdots & \ddots & \vdots & \vdots & \ddots & \vdots \\ \frac{\partial q_s'}{\partial q_1} & \cdots & \frac{\partial q_s'}{\partial q_s} & \frac{\partial q_s'}{\partial p_1} & \cdots & \frac{\partial q_s'}{\partial p_s} \\ \frac{\partial p_1'}{\partial q_1} & \cdots & \frac{\partial p_1'}{\partial q_1} & \frac{\partial p_1'}{\partial p_1} & \cdots & \frac{\partial p_1'}{\partial p_s} \\ \vdots & \ddots & \vdots & \vdots & \ddots & \vdots \\ \frac{\partial p_s'}{\partial q_1} & \cdots & \frac{\partial p_s'}{\partial q_s} & \frac{\partial p_s'}{\partial p_1} & \cdots & \frac{\partial p_s'}{\partial p_s} \end{bmatrix},$$

$$\mathbf{A} = \begin{bmatrix} \mathbf{0}_s & \mathbf{I}_s \\ -\mathbf{I}_s & \mathbf{0}_s \end{bmatrix}, \tag{3}$$

where $\mathbf{I}_s$ is the $s \times s$ identity matrix and $\mathbf{0}_s$ is the $s \times s$ null matrix. Considering, for convenience, a one-particle system in Cartesian coordinates, $\mathbf{MAM}^T$ between $(\mathbf{p},\mathbf{q})$ and $(\mathbf{p}',\mathbf{q}')$ is found to be

$$\mathbf{M} = \begin{bmatrix} \mathbf{I}_3 & \mathbf{0}_3 \\ m\nabla\mathbf{u} & \mathbf{I}_3 \end{bmatrix}, \quad \mathbf{MAM}^T = \begin{bmatrix} \mathbf{0}_3 & \mathbf{I}_3 \\ -\mathbf{I}_3 & m[\nabla\mathbf{u} - (\nabla\mathbf{u})^T] \end{bmatrix}, \tag{4}$$

where

$$\nabla\mathbf{u} = \begin{bmatrix} \frac{\partial u_x}{\partial x} & \frac{\partial u_x}{\partial y} & \frac{\partial u_x}{\partial z} \\ \frac{\partial u_y}{\partial x} & \frac{\partial u_y}{\partial y} & \frac{\partial u_y}{\partial z} \\ \frac{\partial u_z}{\partial x} & \frac{\partial u_z}{\partial y} & \frac{\partial u_z}{\partial z} \end{bmatrix}. \tag{5}$$

A consequence of Eq. (4) is that this transformation would, in general, not be canonical; only in the case of $\nabla\mathbf{u} = (\nabla\mathbf{u})^T$, i.e., elongational flows, would it be canonical. Calculating the Jacobian J between $(\mathbf{p},\mathbf{q})$ and $(\mathbf{p}',\mathbf{q}')$ from the matrix $\mathbf{M}$, it is found from Eq. (1) that

$$J = \frac{\partial(\mathbf{p}',\mathbf{q}')}{\partial(\mathbf{p},\mathbf{q})} = \det(\mathbf{M}) = 1, \tag{6}$$

from which, for an N-particle system, we have $\int d\mathbf{p}_1' \cdots d\mathbf{p}_N' d\mathbf{q}_1' \cdots d\mathbf{q}_N' = \int d\mathbf{p}_1 \cdots d\mathbf{p}_N d\mathbf{q}_1 \cdots d\mathbf{q}_N$. Thus, phase-space volume is conserved through the transformation between $(\mathbf{p},\mathbf{q})$ and $(\mathbf{p}',\mathbf{q}')$, even though the transformation is not canonical. Hereafter, we use a simplified notation for an N-particle system: $\mathbf{p} \equiv \{\mathbf{p}_1,\ldots,\mathbf{p}_N\}$, $\mathbf{q} \equiv \{\mathbf{q}_1,\ldots,\mathbf{q}_N\}$, $\int d\mathbf{p} \equiv \int d\mathbf{p}_1 \cdots d\mathbf{p}_N$, and $\int d\mathbf{q} \equiv \int d\mathbf{q}_1 \cdots d\mathbf{q}_N$.

Although there has been some prior attention to the laboratory momenta, most of the previous work on NEMD algorithms has given the peculiar momenta a special importance in constructing the Hamiltonian, the governing equations of motion, and the distribution function of the nonequilibrium systems. This probably results from the fact that several important physical quantities, such as the temperature and the pressure tensor, are based on the peculiar momenta. However, from the theoretical point of view, the two momenta are equally valid as phase-space variables; that is, the two phase spaces, $(\mathbf{p},\mathbf{q})$ and $(\mathbf{p}',\mathbf{q}')$ should be considered equally valid representations of nonequilibrium physical systems. We shall see below that, whereas the appropriate phase space for the DOLLS algorithm is $(\mathbf{p},\mathbf{q})$, it is $(\mathbf{p}',\mathbf{q}')$ for the p-SLLOD algorithm.

A. DOLLS

The Hamiltonian in the DOLLS algorithm is given by

$$\begin{aligned} H(\mathbf{p},\mathbf{q}) &= \sum_{i=1}^{N} \frac{\mathbf{p}_i^2}{2m_i} + V(\mathbf{q}) + \sum_{i=1}^{N} \mathbf{q}_i\mathbf{p}_i : (\nabla\mathbf{u})^T \\ &= \sum_{i=1}^{N} \frac{1}{2m_i}(\mathbf{p}_i + m_i\mathbf{q}_i\cdot\nabla\mathbf{u})^2 + V(\mathbf{q}) \\ &\quad - \sum_{i=1}^{N} \frac{1}{2} m_i(\mathbf{q}_i\cdot\nabla\mathbf{u})^2, \end{aligned} \tag{7}$$

where $\mathbf{a}\cdot\nabla\mathbf{u} = \Sigma_\alpha a_\alpha \nabla_\alpha u_\upsilon$ and $\mathbf{a}:\mathbf{b} = \Sigma_\alpha \Sigma_\beta a_{\alpha\beta} b_{\beta\alpha}$. The corresponding canonical equations of motion are derived as

$$\begin{aligned} \dot{\mathbf{q}}_i &= \frac{\partial H}{\partial \mathbf{p}_i} = \frac{\mathbf{p}_i}{m_i} + \mathbf{q}_i\cdot\nabla\mathbf{u}, \\ \dot{\mathbf{p}}_i &= -\frac{\partial H}{\partial \mathbf{q}_i} = \mathbf{F}_i - \nabla\mathbf{u}\cdot\mathbf{p}_i, \end{aligned} \tag{8}$$

where $\mathbf{F}_i = -\partial V/\partial\mathbf{q}_i$. As long as the equations of motion correctly represent real physical systems, we can apply the Hamiltonian for many theoretical methodologies.[1,3] In view of the local equilibrium assumption, one can assume that the canonical distribution function $f(\mathbf{p},\mathbf{q})$ of the nonequilibrium system, as a solution of the Liouville theorem $df/dt = 0$, has the form

$$f(\mathbf{p},\mathbf{q})=\frac{\exp\left\{-\frac{1}{k_BT}\left[\Sigma_{i=1}^{N}\frac{\mathbf{p}_i^2}{2m_i}+V(\mathbf{q})+\Sigma_{i=1}^{N}\mathbf{q}_i\mathbf{p}_i:(\nabla\mathbf{u})^T\right]\right\}}{Z}, \tag{9}$$

where the partition function Z is given by

$$Z=\int_{\mathbf{p}}\int_{\mathbf{q}}d\mathbf{p}\,d\mathbf{q}\exp\left\{-\frac{1}{k_BT}\left[\sum_{i=1}^{N}\frac{\mathbf{p}_i^2}{2m_i}+V(\mathbf{q})+\sum_{i=1}^{N}\mathbf{q}_i\mathbf{p}_i:(\nabla\mathbf{u})^T\right]\right\}. \tag{10}$$

Now let us examine the DOLLS algorithm in the phase space $(\mathbf{p}',\mathbf{q}')$. Since the transformation between $(\mathbf{p},\mathbf{q})$ and $(\mathbf{p}',\mathbf{q}')$ does not involve time explicitly, it is natural to take $H'(\mathbf{p}_i',\mathbf{q}_i')=H(\mathbf{p}_i,\mathbf{q}_i)$ with $V'(\mathbf{q}')=V(\mathbf{q})$ and $\partial V'/\partial\mathbf{q}'=\partial V/\partial\mathbf{q}$. Thus, it follows, using the transformation equation (1), that

$$H'(\mathbf{p}',\mathbf{q}')=\sum_{i=1}^{N}\frac{1}{2m_i}\mathbf{p}_i'^2+V'(\mathbf{q}')-\sum_{i=1}^{N}\frac{1}{2}m_i(\mathbf{q}_i'\cdot\nabla\mathbf{u})^2. \tag{11}$$

Assuming the canonical structure of phase space $(\mathbf{p}',\mathbf{q}')$, the equations of motion would be

$$\begin{aligned}\dot{\mathbf{q}}_i'&=\frac{\partial H'}{\partial\mathbf{p}_i'}=\frac{\mathbf{p}_i'}{m_i},\\ \dot{\mathbf{p}}_i'&=-\frac{\partial H'}{\partial\mathbf{q}_i'}=\mathbf{F}_i+m_i\nabla\mathbf{u}\cdot(\mathbf{q}_i'\cdot\nabla\mathbf{u}).\end{aligned} \tag{12}$$

Note that $\partial m_i(\mathbf{q}_i\cdot\nabla\mathbf{u})^2/\partial\mathbf{q}_i$ is not equal to $2m_i\mathbf{q}_i\cdot\nabla\mathbf{u}\cdot\nabla\mathbf{u}$ but to $2m_i\nabla\mathbf{u}\cdot(\mathbf{q}_i\cdot\nabla\mathbf{u})$. Transforming Eq. (12) from $(\mathbf{p}',\mathbf{q}')$ to $(\mathbf{p},\mathbf{q})$, it becomes

$$\begin{aligned}\dot{\mathbf{q}}_i&=\frac{\partial H}{\partial\mathbf{p}_i}=\frac{\mathbf{p}_i}{m_i}+\mathbf{q}_i\cdot\nabla\mathbf{u},\\ \dot{\mathbf{p}}_i&=-\frac{\partial H}{\partial\mathbf{q}_i}=\mathbf{F}_i-\mathbf{p}_i\cdot\nabla\mathbf{u}-m_i\mathbf{q}_i\cdot\nabla\mathbf{u}\cdot\nabla\mathbf{u}+m_i\nabla\mathbf{u}\cdot(\mathbf{q}_i\cdot\nabla\mathbf{u}).\end{aligned} \tag{13}$$

Clearly Eq. (13) is not equivalent to Eq. (8). Therefore H' is a conserved quantity but not a Hamiltonian. This is exactly what is expected from the noncanonical relationship between $(\mathbf{p},\mathbf{q})$ and $(\mathbf{p}',\mathbf{q}')$. To the best of our knowledge, one could not derive the equations of motion of the DOLLS algorithm from any form of $H'(\mathbf{p}',\mathbf{q}')$. Thus, it is concluded that for the DOLLS algorithm there exists a Hamiltonian in phase space $(\mathbf{p},\mathbf{q})$, but only a conserved quantity, not a Hamiltonian, in phase space $(\mathbf{p}',\mathbf{q}')$.

Another subject worthy of consideration is the canonical distribution function. Although $H'(\mathbf{p}',\mathbf{q}')$ is not a Hamiltonian, it is conserved $(dH'/dt=0)$, which can be explicitly verified using Eqs. (11) and (12) or simply from the fact that $H'(\mathbf{p}',\mathbf{q}')=H(\mathbf{p},\mathbf{q})$. The conservative property still guarantees $f'\sim\exp(H'/k_BT)$ as a solution of the Liouville theorem $df'/dt=0$. Therefore, the canonical distribution function and the partition function in phase space $(\mathbf{p}',\mathbf{q}')$ are written as

$$f'(\mathbf{p}',\mathbf{q}')=\frac{\exp\left\{-\frac{1}{k_BT}\left[\Sigma_{i=1}^{N}\frac{1}{2m_i}\mathbf{p}_i'^2+V(\mathbf{q}')-\Sigma_{i=1}^{N}\frac{1}{2}m_i(\mathbf{q}_i'\cdot\nabla\mathbf{u})^2\right]\right\}}{Z'}, \tag{14}$$

where

$$Z'=\int_{\mathbf{p}'}\int_{\mathbf{q}'}d\mathbf{p}'\,d\mathbf{q}'\exp\left\{-\frac{1}{k_BT}\left[\sum_{i=1}^{N}\frac{1}{2m_i}\mathbf{p}_i'^2+V(\mathbf{q}')-\sum_{i=1}^{N}\frac{1}{2}m_i(\mathbf{q}_i'\cdot\nabla\mathbf{u})^2\right]\right\}. \tag{15}$$

However, these forms of $f'(\mathbf{p}',\mathbf{q}')$ and Z' can also be derived by effecting the transformation of $f(\mathbf{p},\mathbf{q})$ and Z using Eq. (1) with the help of the relation $\int d\mathbf{p}'\,d\mathbf{q}'=\int d\mathbf{p}\,d\mathbf{q}$. Thus, we have found one connection between $(\mathbf{p},\mathbf{q})$ and $(\mathbf{p}',\mathbf{q}')$ consistent with a physical point of view.

Next, let us look into the Newtonian dynamics resulting from the DOLLS algorithm, an important characteristic in judging whether a NEMD algorithm is capable of representing physical systems correctly. It is known[2,3] that appropriate time-dependent boundary conditions, such as the Lees-Edwards boundary conditions,[12] together with Newton's equation of motion $m_i\ddot{\mathbf{q}}_i=\mathbf{F}_i$, are sufficient to generate nonequilibrium states correctly. Hereafter, it is assumed that a nonequilibrium system of interest is equipped with proper boundary conditions, whether time dependent or not, and a NEMD algorithm therefore must be consistent with Newton's equation. From the equations of motion (8) of the DOLLS algorithm, it is found that

$$m_i\ddot{\mathbf{q}}_i=\mathbf{F}_i-\boldsymbol{\nabla}\mathbf{u}\cdot\mathbf{p}_i+\mathbf{p}_i\cdot\boldsymbol{\nabla}\mathbf{u}+m_i\mathbf{q}_i\cdot\boldsymbol{\nabla}\mathbf{u}\cdot\boldsymbol{\nabla}\mathbf{u}, \tag{16}$$

which is not consistent with Newton's equation. Therefore, it is concluded that the DOLLS algorithm, in general, would not correctly represent nonequilibrium systems.

Let us specifically consider two practically important cases. The external velocity fields for simple shear flow and elongational flows are given by

$$\boldsymbol{\nabla}\mathbf{u}=\begin{bmatrix}0 & \dot{\gamma} & 0\\ 0 & 0 & 0\\ 0 & 0 & 0\end{bmatrix} \quad \text{for simple shear flow,} \tag{17a}$$

$$\boldsymbol{\nabla}\mathbf{u}=\begin{bmatrix}\dot{\epsilon}_{xx} & 0 & 0\\ 0 & \dot{\epsilon}_{yy} & 0\\ 0 & 0 & \dot{\epsilon}_{zz}\end{bmatrix} \quad \text{for elongational flow,} \tag{17b}$$

where $\dot{\gamma}$ denotes shear rate, $\dot{\epsilon}_{xx}$ elongational rate of the xx component, and so on. PEF is described by $\dot{\epsilon}_{xx}=-\dot{\epsilon}_{yy}=\dot{\epsilon}$ and $\dot{\epsilon}_{zz}=0$ in Eq. (17). Since the last term on the right-hand side (RHS) in Eq. (16) vanishes for simple shear flow, the resulting evolution equation is written as

$$m_i\ddot{\mathbf{q}}_i=\mathbf{F}_i-\boldsymbol{\nabla}\mathbf{u}\cdot\mathbf{p}_i+\mathbf{p}_i\cdot\boldsymbol{\nabla}\mathbf{u}. \tag{18}$$

For elongational flows, the second and third terms on the RHS in Eq. (16) vanish together, and it follows that

$$m_i\ddot{\mathbf{q}}_i=\mathbf{F}_i+m_i\mathbf{q}_i\cdot\boldsymbol{\nabla}\mathbf{u}\cdot\boldsymbol{\nabla}\mathbf{u}. \tag{19}$$

Since neither Eq. (18) nor Eq. (19) is consistent with Newton's equation of motion, we conclude that the DOLLS dynamics would not be capable of representing either shear flow or elongational flows. This explains why the DOLLS algorithm gives incorrect results for shear flow as mentioned previously and which led to the SLLOD algorithm.

B. SLLOD

The equations of motion of the SLLOD algorithm are given by

$$\begin{aligned}\dot{\mathbf{q}}_i&=\frac{\mathbf{p}_i}{m_i}+\mathbf{q}_i\cdot\boldsymbol{\nabla}\mathbf{u},\\ \dot{\mathbf{p}}_i&=\mathbf{F}_i-\mathbf{p}_i\cdot\boldsymbol{\nabla}\mathbf{u}.\end{aligned} \tag{20}$$

Note that in the case of $\boldsymbol{\nabla}\mathbf{u}=(\boldsymbol{\nabla}\mathbf{u})^T$, Eq. (20) would be equal to Eq. (8) and the SLLOD algorithm would be the same as the DOLLS algorithm. Unfortunately, there has not been found a Hamiltonian to generate the equations of motion (20) of the SLLOD algorithm in any phase space, either $(\mathbf{p},\mathbf{q})$ or $(\mathbf{p}',\mathbf{q}')$, which is regarded as a weak point in the algorithm. [Tuckerman *et al.*[9] showed the existence of a restricted Hamiltonian under a special condition $\boldsymbol{\nabla}\mathbf{u}\cdot\boldsymbol{\nabla}\mathbf{u}=(\boldsymbol{\nabla}\mathbf{u}\cdot\boldsymbol{\nabla}\mathbf{u})^T$.] So, we shall only discuss the evolution equations generated by the SLLOD algorithm. From Eq. (20), it is readily shown that

$$m_i\ddot{\mathbf{q}}_i=\mathbf{F}_i+m_i\mathbf{q}_i\cdot\boldsymbol{\nabla}\mathbf{u}\cdot\boldsymbol{\nabla}\mathbf{u}, \tag{21}$$

which again is not consistent with Newton's equations. Therefore, like the DOLLS algorithm, the SLLOD algorithm would not, in general, represent nonequilibrium states correctly.

It would seem to be a disadvantage of the SLLOD algorithm that it fails to satisfy Newton's equation in arbitrary velocity gradient fields. Consequently, the frame of reference of the SLLOD algorithm is *not* an inertial reference frame (except in special cases such as planar Couette flow), and, in our opinion, this is a disadvantage of this algorithm. After all, the real laboratory experiment is conducted in an inertial frame of reference. It is not clear how the SLLOD stress tensor calculation translates from the noninertial reference frame of the simulation to the inertial reference frame of the experiment.

For simple shear flow, Eq. (21) becomes

$$m_i\ddot{\mathbf{q}}_i=\mathbf{F}_i, \tag{22}$$

which, of course, is identical to Newton's equation. Therefore, the SLLOD algorithm is capable of representing sheared fluids. This is one reason why the SLLOD algorithm, rather than DOLLS, has given physically reasonable results for nonequilibrium systems under shear at higher values of the shear rate. However, for elongational flows where the second term on the RHS of Eq. (21) does not vanish, the SLLOD algorithm is not expected to give correct results because of this inconsistency with Newton's equation of motion.

C. *p*-SLLOD

Now let us examine the p-SLLOD algorithm. There exists a Hamiltonian in the p-SLLOD algorithm, not in phase space $(\mathbf{p},\mathbf{q})$ but in $(\mathbf{p}',\mathbf{q}')$;

$$H'(\mathbf{p}',\mathbf{q}')=\sum_{i=1}^{N}\frac{1}{2m_i}\mathbf{p}_i'^2+V'(\mathbf{q}'), \tag{23}$$

from which the canonical equations of motion are derived as

$$\begin{aligned}\dot{\mathbf{q}}_i'&=\frac{\partial H'}{\partial\mathbf{p}_i'}=\frac{\mathbf{p}_i'}{m_i},\\ \dot{\mathbf{p}}_i'&=-\frac{\partial H'}{\partial\mathbf{q}_i'}=\mathbf{F}_i.\end{aligned} \tag{24}$$

Expressing Eq. (24) in the phase space $(\mathbf{p},\mathbf{q})$, it is found that

$$\begin{aligned}\dot{\mathbf{q}}_i&=\frac{\mathbf{p}_i}{m_i}+\mathbf{q}_i\cdot\boldsymbol{\nabla}\mathbf{u},\\ \dot{\mathbf{p}}_i&=\mathbf{F}_i-\mathbf{p}_i\cdot\boldsymbol{\nabla}\mathbf{u}-m_i\mathbf{q}_i\cdot\boldsymbol{\nabla}\mathbf{u}\cdot\boldsymbol{\nabla}\mathbf{u}.\end{aligned} \tag{25}$$

With the conserved Hamiltonian H', the canonical distribution function and the partition function are written as follows:

$$f'(\mathbf{p}',\mathbf{q}')=\frac{\exp\left\{-\frac{1}{k_BT}\left[\Sigma_{i=1}^{N}\frac{1}{2m_i}\mathbf{p}_i'^2+V(\mathbf{q}')\right]\right\}}{Z'}, \tag{26}$$

where

$$Z'=\int_{\mathbf{p}'}\int_{\mathbf{q}'}d\mathbf{p}'\,d\mathbf{q}'\exp\left\{-\frac{1}{k_BT}\left[\sum_{i=1}^{N}\frac{1}{2m_i}\mathbf{p}_i'^2+V(\mathbf{q}')\right]\right\}. \tag{27}$$

Note that the *p*-SLLOD algorithm would reduce to the SLLOD algorithm in the case of $\nabla\mathbf{u}\cdot\nabla\mathbf{u}=0$, i.e., simple shear flow.

Now let us analyze the *p*-SLLOD algorithm in phase space $(\mathbf{p},\mathbf{q})$ with $H(\mathbf{p}_i,\mathbf{q}_i)=H'(\mathbf{p}_i',\mathbf{q}_i')$ as we did in the DOLLS algorithm:

$$H(\mathbf{p},\mathbf{q})=\sum_{i=1}^{N}\frac{1}{2m_i}(\mathbf{p}_i+m_i\mathbf{q}_i\cdot\nabla\mathbf{u})^2+V(\mathbf{q}). \tag{28}$$

Constructing the canonical equations of motion in phase space $(\mathbf{p},\mathbf{q})$, we see

$$\begin{aligned}\dot{\mathbf{q}}_i&=\frac{\partial H}{\partial\mathbf{p}_i}=\frac{\mathbf{p}_i}{m_i}+\mathbf{q}_i\cdot\nabla\mathbf{u},\\ \dot{\mathbf{p}}_i&=-\frac{\partial H}{\partial\mathbf{q}_i}=\mathbf{F}_i-\nabla\mathbf{u}\cdot\mathbf{p}_i-m_i\nabla\mathbf{u}\cdot(\mathbf{q}_i\cdot\nabla\mathbf{u}).\end{aligned} \tag{29}$$

Equation (29) is not equivalent to Eq. (25). The reason for this apparent discrepancy was discussed by Edwards and Dressler:[10] in phase space $(\mathbf{p},\mathbf{q})$, the equations of motion are not of canonical form. Thus Eqs. (29) are not correct equations of motion for the *p*-SLLOD system. This is exactly the opposite of the case in the DOLLS algorithm: in DOLLS, the phase space $(\mathbf{p},\mathbf{q})$ has canonical equations of motion, whereas in *p*-SLLOD, phase space $(\mathbf{p}',\mathbf{q}')$ has canonical equations of motion.

Using the same procedure as in the DOLLS algorithm, the canonical distribution function and the corresponding partition function are found to be

$$f(\mathbf{p},\mathbf{q})=\frac{\exp\left\{-\frac{1}{k_BT}\left[\Sigma_{i=1}^{N}\frac{1}{2m_i}(\mathbf{p}_i+m_i\mathbf{q}_i\cdot\nabla\mathbf{u})^2+V(\mathbf{q})\right]\right\}}{Z}, \tag{30}$$

where

$$Z=\int_{\mathbf{p}}\int_{\mathbf{q}}d\mathbf{p}\,d\mathbf{q}\exp\left\{-\frac{1}{k_BT}\left[\sum_{i=1}^{N}\frac{1}{2m_i}(\mathbf{p}_i+m_i\mathbf{q}_i\cdot\nabla\mathbf{u})^2+V(\mathbf{q})\right]\right\}. \tag{31}$$

Therefore, $f(\mathbf{p},\mathbf{q})$ and Z are equal to $f'(\mathbf{p}',\mathbf{q}')$ and Z', respectively, as in the DOLLS algorithm.

Next let us derive the Newtonian dynamics dictated by the *p*-SLLOD algorithm. From Eq. (25) it is found to be

$$m_i\ddot{\mathbf{q}}_i=\mathbf{F}_i. \tag{32}$$

This is exactly Newton's equation, which is the required form for a NEMD algorithm; thus, the *p*-SLLOD algorithm will make a physically correct prediction for *any* flow. This fact could be deduced from the rigorously canonical structure of Eq. (24) in phase space $(\mathbf{p}',\mathbf{q}')$ without involving any velocity-dependent nonequilibrium term, unlike the DOLLS algorithm in its phase space $(\mathbf{p},\mathbf{q})$.

To summarize this section, the DOLLS algorithm has a Hamiltonian in phase space $(\mathbf{p},\mathbf{q})$ and a conserved quantity but not a Hamiltonian in $(\mathbf{p}',\mathbf{q}')$. It is not capable of representing nonequilibrium systems either for shear or elongational flows because its equations of motion are inconsistent with Newton's equation. On the other hand, the SLLOD algorithm does not have a Hamiltonian in either $(\mathbf{p},\mathbf{q})$ or $(\mathbf{p}',\mathbf{q}')$, but it is capable of representing nonequilibrium systems with shear flow but not elongational flows because in shear flow its equations of motion are consistent with Newton's equation. Finally, the *p*-SLLOD algorithm has canonical form in phase space $(\mathbf{p}',\mathbf{q}')$ and a noncanonical form in $(\mathbf{p},\mathbf{q})$, and it is capable of representing nonequilibrium systems for any flow field because its equations of motion are, in general, consistent with Newton's equation. In short, the *p*-SLLOD algorithm is considered the most satisfactory among the existing NEMD algorithms, and it is for this reason that we employ the term proper-SLLOD.

III. EVOLUTION OF THE TOTAL LINEAR MOMENTUM

From our analysis of the three NEMD algorithms in the peculiar and laboratory frames above, we understand the origin of the differences among them and we have a firm, physical basis for greater confidence in the *p*-SLLOD algorithm. Let us now examine the evolution of the total linear momentum of a system resulting from the equations of motion of each NEMD algorithm. Recall that it is the exponential growth of the total linear momentum of PEF with the SLLOD algorithm that was observed by Todd and Daivis.[8] As already mentioned, for simple shear flow the SLLOD and the *p*-SLLOD algorithms are equivalent, and for elongational flows the DOLLS and the SLLOD algorithms are equivalent. Summing over all the particles of a system and observing Newton's third law $[\Sigma_i\mathbf{F}_i=\mathbf{0}]$, the equations of motion for the total momentum of each algorithm are written as

$$\begin{aligned}\dot{Q}_\alpha&=P_\alpha+\sum_\beta Q_\beta\nabla_\beta u_\alpha,\\ \dot{P}_\alpha&=-\sum_\beta\nabla_\alpha u_\beta P_\beta \quad \text{for DOLLS,}\end{aligned} \tag{33}$$

$$\begin{aligned}\dot{Q}_\alpha&=P_\alpha+\sum_\beta Q_\beta\nabla_\beta u_\alpha,\\ \dot{P}_\alpha&=-\sum_\beta P_\beta\nabla_\beta u_\alpha \quad \text{for SLLOD,}\end{aligned} \tag{34}$$

$$\begin{aligned}\dot{Q}_\alpha&=P_\alpha+\sum_\beta Q_\beta\nabla_\beta u_\alpha,\\ \dot{P}_\alpha&=-\sum_\beta P_\beta\nabla_\beta u_\alpha-\sum_\beta\sum_\nu Q_\beta\nabla_\beta u_\nu\nabla_\nu u_\alpha \quad \text{for } p\text{-SLLOD.}\end{aligned} \tag{35}$$

In these expressions, the total linear momentum is defined as $P_\alpha=\Sigma_i p_{\alpha i}$ and the first moment as $Q_\alpha=\Sigma_i m_i q_{\alpha i}$. Here, Greek subscripts represent *x*, *y*, and *z* components.

First, we consider simple shear and then elongational flow fields, as described by Eq. (17). For simple shear flow, the evolution equations of the total linear momentum of each system are found to be

$$P_\alpha(t)=P_\alpha(t_0)-\delta_{\alpha y}\dot{\gamma}P_x(t_0)(t-t_0) \quad \text{for DOLLS,} \tag{36}$$

$$P_\alpha(t)=P_\alpha(t_0)-\delta_{\alpha x}\dot{\gamma}P_y(t_0)(t-t_0) \quad \text{for SLLOD and } p\text{-SLLOD,} \tag{37}$$

where the Kronecker delta $\delta_{\alpha\beta}$ is equal to 1 for $\alpha=\beta$ and 0 otherwise. Therefore, the total linear momentum of the system is at most linearly dependent on time for all of the NEMD algorithms.

For elongational flows, it follows that

$$P_\alpha(t)=P_\alpha(t_0)\exp[-\dot{\epsilon}_{\alpha\alpha}(t-t_0)] \quad \text{for DOLLS and SLLOD,} \tag{38}$$

$$P_\alpha(t)=P_\alpha(t_0)-\dot{\epsilon}_{\alpha\alpha}[P_\alpha(t_0)+\dot{\epsilon}_{\alpha\alpha}Q_\alpha(t_0)](t-t_0) \quad \text{for } p\text{-SLLOD.} \tag{39}$$

From Eq. (38), we see that the total linear momentum is exponentially dependent on time in the cases of the DOLLS and the SLLOD algorithms. Therefore, for $\dot{\epsilon}_{\alpha\alpha}<0$, an exponential growth of the total linear momentum will occur in the α direction unless the initial total momentum is exactly equal to zero, which would never be achieved in computer simulations because of truncation error. This is what Todd and Daivis[8] observed in PEF simulations with the SLLOD algorithm. From Eq. (39), when using the p-SLLOD algorithm, however, the total momentum depends only linearly on time, as in simple shear flow, and, therefore, we no longer have the instability problem that occurs in the SLLOD algorithm. These results seem naturally related to the intrinsic shortcomings of the DOLLS and SLLOD algorithms and the universality of the p-SLLOD algorithm, as described in Sec. II. With this observation, we have conducted NEMD simulations for planar elongational flow using the p-SLLOD algorithm and compared the results with those of the SLLOD algorithm. The results are presented in Sec. V.

IV. SIMULATION STRATEGY

In this section we detail our strategy for simulation of PEF. Readers primarily interested in the theoretical aspects of our work may skip this section without loss; however, as we note below, reliable, practical simulations of PEF require care to avoid artifacts.

For our nvt NEMD simulations of PEF [$\dot{\epsilon}_{xx}=-\dot{\epsilon}_{yy}=\dot{\epsilon}$ and $\dot{\epsilon}_{zz}=0$ in Eq. (17)], the Nosé-Hoover thermostat[13–15] was chosen to maintain the system temperature constant. We note that all thermostats, except the configurational thermostat of Delhommelle and Evans,[16,17] result in artifacts at very high shear rates (e.g., $\dot{\gamma}>1$). To the best of our knowledge, the thermostat artifacts in PEF have not been explored, but are not expected to be significant because of the absence of vorticity; this may be confirmed in the ongoing work. The p-SLLOD algorithm, incorporating the Nosé-Hoover thermostat, is written as[3,18]

$$\begin{aligned}
\dot{\mathbf{q}}_i&=\frac{\mathbf{p}_i}{m_i}+\mathbf{q}_i\cdot\nabla\mathbf{u},\\
\dot{\mathbf{p}}_i&=\mathbf{F}_i-\mathbf{p}_i\cdot\nabla\mathbf{u}-m_i\mathbf{q}_i\cdot\nabla\mathbf{u}\cdot\nabla\mathbf{u}-\frac{p_\eta}{Q}\mathbf{p}_i,\\
\dot{\eta}&=\frac{p_\eta}{Q},\\
\dot{p}_\eta&=\sum_{i=1}^{N}\frac{\mathbf{p}_i^2}{m_i}-DNk_BT,
\end{aligned} \tag{40}$$

where D denotes dimensionality, N the number of particles, T the temperature, and k_B the Boltzmann constant. Here η and p_η are coordinatelike and momentumlike variables of the Nosé-Hoover thermostat, respectively, and $Q=DNk_BT\tau^2$ is the mass parameter of the thermostat. In the present work, all of the system and simulation conditions have been set as in the previous works[6–8] for comparison purposes. We studied the Weeks–Chandler–Andersen (WCA) fluid whose potential model in reduced units is given by[19]

$$\phi(r)=\begin{cases}4(r^{-12}-r^{-6})+1 & \text{for } r<2^{1/6}\\ 0 & \text{for } r>2^{1/6}\end{cases}. \tag{41}$$

Note that all the parameters, variables, and physical quantities presented in this paper are expressed in reduced units (see Appendix B in Ref. 20).

NEMD simulations were performed at temperature $T=0.722$ and number density $\rho=0.8442$. A system of 500 WCA particles was used in simulations, for which the time step was chosen as 0.001 925 and the velocity Verlet integration scheme was employed. The relaxation time parameter τ of the Nosé-Hoover thermostat was set equal to 0.096. As for the KRBCs, we chose the Hencky strain $\epsilon_p\approx0.9624$ and the initial orientation angle of the simulation box $\theta_0\approx31.718°$, which are obtained by setting $k=3$, $N_{11}=2$, and $N_{12}=-1$ in Ref. 5. The time period t_p for KRBCs is determined from $\epsilon_p=\dot{\epsilon}t_p$. In applying KRBCs, we followed the efficient procedure suggested by Todd and Daivis.[7] Here we will not describe the details of either KRBCs or the Todd-Daivis procedure to avoid unnecessary repetition, and refer readers to the original papers.[4,5,7]

Now let us mention two crucial simulation details in implementing the p-SLLOD algorithm for PEF. The first is that, since the momentum equation (25) involves the position of a particle (not only the relative distance between particles), we should not apply the periodic boundary conditions (PBCs) (Ref. 20) to the position of the particle used in Eq. (25). Instead, we should retain the particle position without applying PBCs during each time period t_p and use it in the momentum equation. This is a natural procedure in the p-SLLOD algorithm since to apply PBCs is to violate the very rule of evolution of the trajectory underlying the p-SLLOD algorithm. Of course, we still use the minimum image convention[20] when calculating force. The only place we apply PBCs is at the end of each time period, at which time the lattice vectors or boundaries of the simulation cell transform back into the initial ones according to KRBCs.

The second simulation detail to be considered comes from the fact that the time-evolution equation of the total linear momentum of the system (39) depends on two components for its slope; one is the initial total momentum $P_\alpha(t_0)$ and the other the initial first moment $Q_\alpha(t_0)$. Since the KRBCs applied at the end of the time period make a transformation in the center of mass of the system, the value of $Q_\alpha(t_0)$ changes from one period to the next. As a result, a large value of the initial slope for the next time period may result, and this would make the system unstable. In order to prevent the problem, we need to adjust the initial slope at each time period without making any artificial perturbation to the dynamics of the system. The smaller the slope, the more stable is the evolution of the system. This has been easily achieved by a uniform translation of particles in space as follows:

$$q_{\alpha i}(0,j) = q_{\alpha i}(t_p, j-1) + C_\alpha(j), \tag{42}$$

where

$$C_\alpha(j) = -\frac{P_\alpha(t_p, j-1) + \dot{\epsilon}_{\alpha\alpha} Q_\alpha(t_p, j-1)}{\dot{\epsilon}_{\alpha\alpha} \sum_{i=1}^{N} m_i}. \tag{43}$$

Here the integer j is the number of time periods. This procedure effectively re-zeros the linear coefficient in Eq. (39) at the beginning of each time period. Since this procedure merely translates the coordinate system of the position vectors and does not affect the equations of motion, the Newtonian evolution equations and the resultant trajectory are not affected. To validate that this procedure does not disturb the evolution of the system, we have checked the evolution of the internal energy and pressure tensor (see Fig. 3 below).

V. RESULTS AND DISCUSSION

In this section we present results of our N-V-T NEMD simulations of PEF. First, we show the evolution of the y component of the linear momentum under both the SLLOD and p-SLLOD algorithms to reproduce the exponential growth presented by Todd and Daivis[8] and to demonstrate its absence with the p-SLLOD algorithm. We also examine the evolution of the internal energy per particle for both long and short times to demonstrate the absence of artifacts with the p-SLLOD algorithm. Finally, we show that omission of a necessary term from the SLLOD algorithm for PEF results in incorrect predictions of the internal energy, the stress tensor, and the elongational viscosity. Although the errors are large only at very high strain rates, nevertheless, for purposes of testing theories of PEF it is vital that NEMD simulations be reliable.

In N-V-T NEMD simulations, due to the interaction of a thermostat with the system, the evolution of the total linear momentum would not exactly follow Eq. (38) in the SLLOD and Eq. (39) in the p-SLLOD algorithms. As pointed out by Todd and Daivis,[8] at high elongational rate, where a large effect of the thermostat is expected, the exponential growth of the total y momentum does not occur in the SLLOD algorithm. However, at low elongational rate where the effect of the thermostat is negligible, the exponential growth of the total y momentum is observed. That is, the exponential growth in the SLLOD algorithm becomes more substantial as elongational rate decreases. It is therefore sufficient for comparison purpose to show the results only for a low elongational rate.

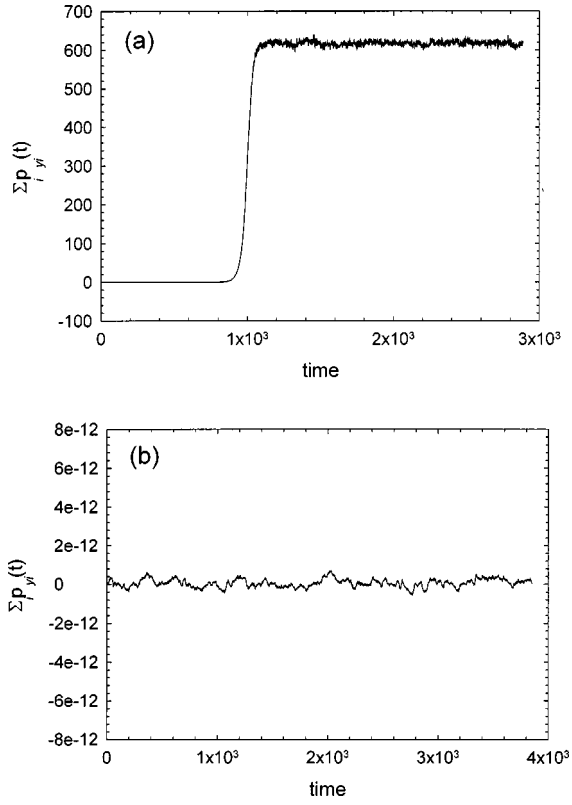

FIG. 1. Evolution of the total linear momentum of system in the y direction with time at $\dot{\epsilon}=0.05$: (a) using the SLLOD algorithm, (b) using the p-SLLOD algorithm.

Figures 1(a) and 1(b) show the evolution of the total y momentum of the SLLOD and that of the p-SLLOD algorithm at $\dot{\epsilon}=0.05$. Figure 1(a) is essentially the same result as that of Todd and Daivis[8] when using the SLLOD algorithm. However, by using the p-SLLOD algorithm, as shown in Fig. 1(b), we observe a stable evolution of the total y momentum instead of the exponential growth. Figure 2 presents the corresponding evolution of the internal energy per particle. The internal energy E_{int} and the pressure tensor $\mathbf{P}$ of our results are calculated over all particles in the system by the conventional equations:

$$E_{\text{int}} = \left\langle \sum_{i=1}^{N} \frac{\mathbf{p}_i^2}{2m_i} + V(\mathbf{q}) \right\rangle, \tag{44}$$

$$\mathbf{P} = \left\langle \frac{1}{V_s} \sum_{i=1}^{N} \left(\frac{\mathbf{p}_i \mathbf{p}_i}{m_i} + \mathbf{q}_i \mathbf{F}_i \right) \right\rangle, \tag{45}$$

where V_s is the system volume. The angular brackets denote the average over the trajectory of the system (see Appendix B for more precise physical meaning of E_{int} and $\mathbf{P}$). As shown in Fig. 2(a), the exponential growth of the total y momentum in the case of the SLLOD algorithm causes an undesirable phase transition, which does not happen in case of the p-SLLOD algorithm, as shown in Fig. 2(b).

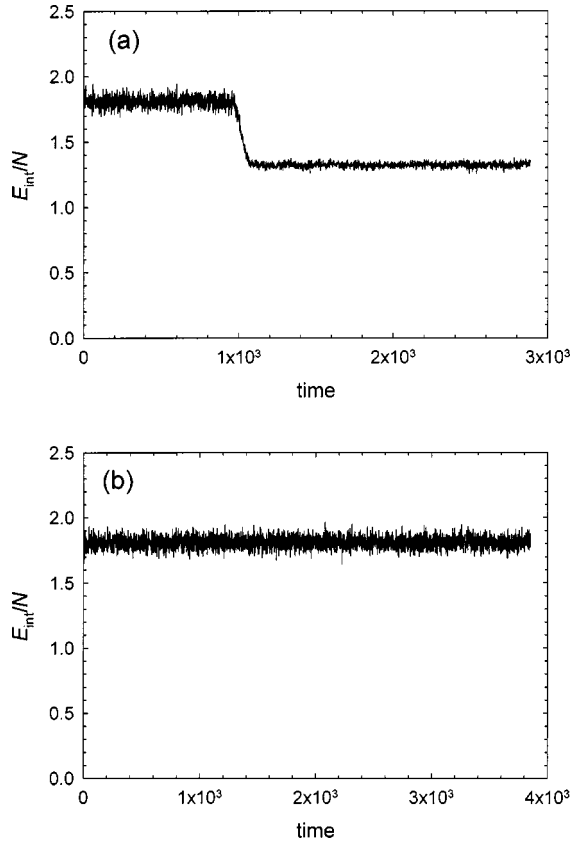

FIG. 2. Evolution of the internal energy per particle with time at $\dot{\epsilon}=0.05$: (a) using the SLLOD algorithm, (b) using the p-SLLOD algorithm.

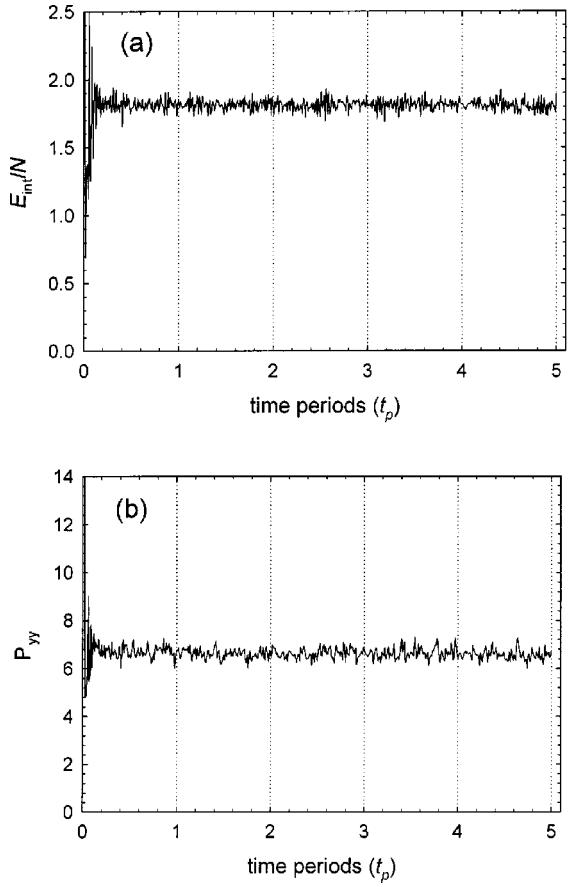

FIG. 3. Close up of evolutions of (a) internal energy per particle and (b) pressure tensor during each time periods (t_p) at $\dot{\epsilon}=0.05$ using the p-SLLOD algorithm.

These results directly demonstrate the stability and correctness of the p-SLLOD algorithm for PEF. To verify that there is no unacceptable discontinuity during the evolution due to the KRBCs together with our simulation strategy, we have looked more closely into the internal energy and the pressure tensor at small time periods. The results are shown in Fig. 3. For the pressure tensor, we have included only P_{yy} for clarity. As shown in the figure, there is no perceptible discontinuity at each time period. We now conclude that using the p-SLLOD algorithm eliminates the aphysical phenomena that occur in the SLLOD algorithm.

Finally, in Fig. 4, we have compared the results of the SLLOD algorithm and those of the p-SLLOD algorithm (the numerical values including statistical uncertainties of our results are shown in Table I for the SLLOD and Table II for the p-SLLOD algorithm). The elongational rates were chosen to be the same as those in Ref. 6, where the system was composed of 108 WCA particles with the Gaussian thermostat.[3] The numerical values of the results in Ref. 6 overall appear to be smaller than ours for the SLLOD algorithm. The difference between the two SLLOD results is perhaps due to the fact that the results from Ref. 6 used only 108 particles, shorter simulations, and/or a different choice of thermostat. (Again, we recognize that both the Gaussian and Nosé thermostats can show artifacts at strain rates greater than one. However, the thermostat cannot explain the difference between our SLLOD and p-SLLOD results since we used the same thermostat for both algorithms.)

At low elongational rates, the results of the p-SLLOD algorithm are similar to those of the SLLOD algorithm within statistical uncertainties. However, as elongational rate increases, the difference becomes larger. This is actually to be expected to a certain degree, considering the difference in the equations of motion between the SLLOD [Eq. (20)] and the p-SLLOD [Eq. (25)] algorithms; the SLLOD algorithm neglects the term that depends quadratically on the external velocity field.

VI. CONCLUSIONS

In this work, we have demonstrated the capabilities of the p-SLLOD algorithm for planar elongational flow and elucidated the fundamental causes of errors and artifacts previously produced with the SLLOD algorithm for PEF. By using the p-SLLOD algorithm, we no longer encounter the aphysical phenomena that were observed in simulations using the SLLOD algorithm. The p-SLLOD algorithm can also be applied to any flow field since it has a perfect canonical structure without any velocity-dependent nonequilibrium term in phase space $(\mathbf{p}',\mathbf{q}')$ and thus satisfies Newton's equation of motion.

ACKNOWLEDGMENTS

This work was supported by the Division of Materials Sciences and Engineering of the U.S. Department of Energy (DOE) at Oak Ridge National Laboratory (ORNL) and

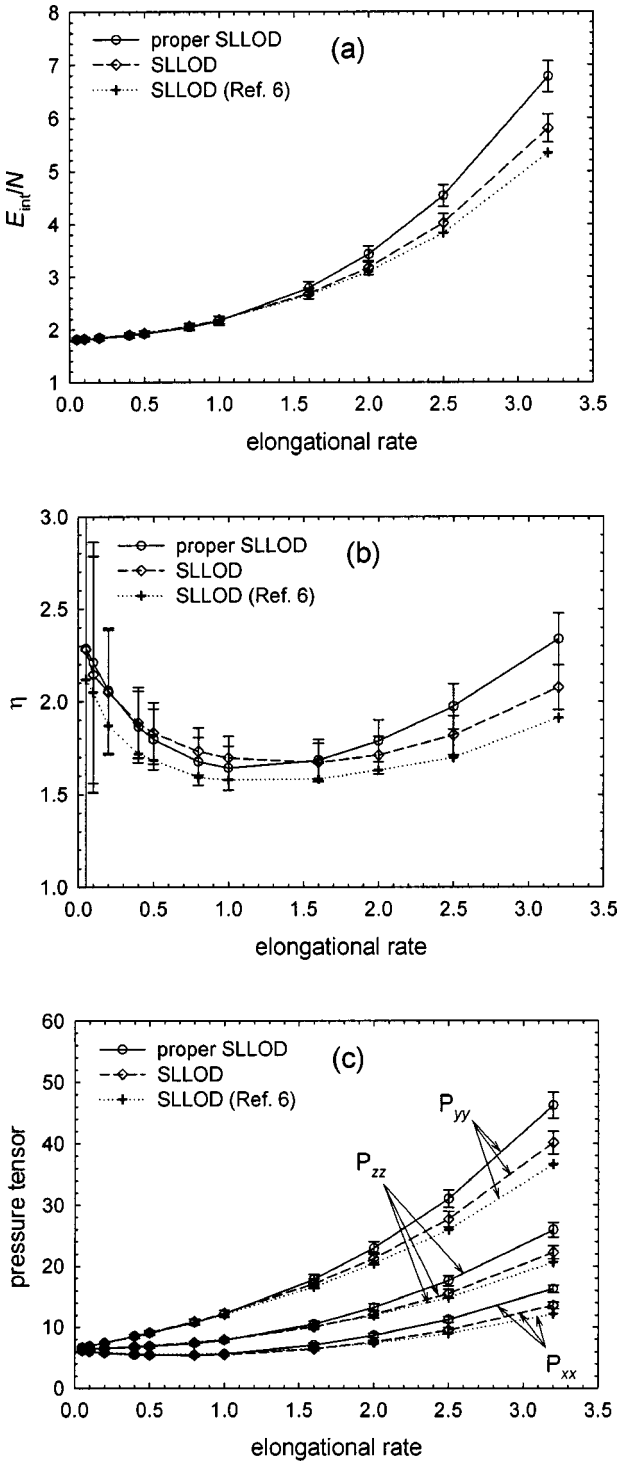

FIG. 4. Comparison of NEMD results between the SLLOD and the p-SLLOD algorithms: (a) internal energy per particle, (b) elongational viscosity, (c) pressure tensor.

through a subcontract at the University of Tennessee. ORNL is operated for the DOE by UT-Battelle, LLC, under Contract No. DE-AC0500OR22725.

APPENDIX A: THE INTERNAL ENERGY IN THE *p*-SLLOD ALGORITHM IN MOVING COORDINATES

In the main body of this paper, the respective NEMD algorithms were examined from the perspective of mechanical consistency; i.e., the algorithms were discussed in terms of Hamiltonian and Newtonian mechanics. In the appendices, we examine them from the perspective of thermodynamic consistency.

In order to understand thoroughly the nature of the p-SLLOD algorithm, it is necessary to investigate the relationships between the laboratory and convecting reference frames used in its derivation. The easiest way to develop this understanding is to consider the laboratory reference frame to be totally flow-free, i.e., $\nabla\mathbf{u}=\mathbf{0}$. Consequently, the equations of motion in this frame can be confidently expressed as Hamilton's equations, and molecular dynamics simulations yield the system properties.

Denoting phase space in the laboratory frame as $(\mathbf{q}',\mathbf{p}')$, the equations of motion are

$$\dot{\mathbf{q}}_i' = \frac{\mathbf{p}_i'}{m_i}, \tag{A1}$$

$$\dot{\mathbf{p}}_i' = \mathbf{F}_i', \tag{A2}$$

and the Hamiltonian is

$$H'(\mathbf{q}',\mathbf{p}') = \sum_{i=1}^{N} \frac{\mathbf{p}_i'\cdot\mathbf{p}_i'}{2m_i} + V(\mathbf{q}'). \tag{A3}$$

It is obvious that the Hamiltonian quantifies the internal energy of the system and also that

$$\frac{dH'}{dt} = 0. \tag{A4}$$

Furthermore, the pressure tensor is calculated through the standard expression

$$\mathbf{P}' = \left\langle \frac{1}{V}\sum_{i=1}^{N}\left(\frac{\mathbf{p}_i'\mathbf{p}_i'}{m_i} + \mathbf{q}_i'\mathbf{F}_i'\right)\right\rangle. \tag{A5}$$

So far, there can be no doubt as to the accuracy of the description of this system. The questions arise when the velocity gradient is nonzero. Let us now examine this problem using a reasoning not commonly employed in NEMD studies. Instead of imposing a nonzero velocity gradient on the system, let us merely transform the laboratory momenta coordinates into coordinates that move *as if* a nonzero velocity gradient were present. These new coordinates can then be viewed as moving with a position-dependent velocity relative to the laboratory frame.

To see the consequences of this point of view, consider a Taylor series expansion of an unspecified velocity field $\mathbf{v}$ in the neighborhood of the origin of a given set of spatial coordinates:

$$\mathbf{v} = \mathbf{v}_0 + \mathbf{q}\cdot\nabla\mathbf{v} + \tfrac{1}{2}\mathbf{q}\mathbf{q}:\nabla\nabla\mathbf{v} + \cdots. \tag{A6}$$

If we linearize the velocity field by neglecting the higher order terms (which vanish anyway for homogeneous flow fields), then this expression allows us to connect the laboratory momenta coordinates with ''peculiar'' momenta coordinates, which move at a constant, position-dependent velocity of $\mathbf{q}_i\cdot\nabla\mathbf{u}$. Consequently, the momenta and positions in the moving coordinates $(\mathbf{q},\mathbf{p})$ are related to the laboratory momenta and positions through the transformations

TABLE I. NEMD simulation results using the SLLOD algorithm. Here, elongational viscosity η is calculated as $(P_{yy}-P_{xx})/4\dot{\epsilon}$. The values in parentheses represent statistical uncertainties. All the results, except those at $\dot{\epsilon}=0.05$, 0.1, and 0.2 due to the phase transition, are obtained from the total simulation time, $t=3850$, corresponding to 2×10^6 time steps with a time step of 0.001 925.

$\dot{\epsilon}$	E_{int}/N	P_{xx}	P_{yy}	P_{zz}	η
0.0	1.809(0.040)	6.397(0.205)	6.396(0.204)	6.397(0.203)	N/A
0.05	1.812(0.041)	6.185(0.198)	6.641(0.214)	6.420(0.205)	2.280(1.290)
0.1	1.818(0.042)	6.030(0.192)	6.889(0.227)	6.448(0.217)	2.147(0.638)
0.2	1.838(0.042)	5.790(0.181)	7.431(0.250)	6.536(0.208)	2.051(0.337)
0.4	1.895(0.046)	5.505(0.179)	8.522(0.303)	6.776(0.228)	1.886(0.191)
0.5	1.930(0.049)	5.426(0.180)	9.086(0.337)	6.916(0.236)	1.830(0.166)
0.8	2.065(0.059)	5.378(0.191)	10.92(0.434)	7.468(0.273)	1.731(0.127)
1.0	2.181(0.069)	5.487(0.205)	12.27(0.514)	7.946(0.308)	1.695(0.117)
1.6	2.681(0.104)	6.429(0.266)	17.13(0.781)	10.06(0.441)	1.671(0.104)
2.0	3.171(0.134)	7.543(0.321)	21.23(0.989)	12.10(0.553)	1.710(0.103)
2.5	4.019(0.179)	9.507(0.397)	27.68(1.281)	15.50(0.732)	1.818(0.106)
3.2	5.804(0.263)	13.58(0.545)	40.16(1.857)	22.26(1.055)	2.077(0.121)

$$\mathbf{q}_i' \to \mathbf{q}_i, \quad \mathbf{p}_i' \to \mathbf{p}_i + m_i \mathbf{q}_i \cdot \nabla \mathbf{u}. \tag{A7}$$

In this new framework, the Hamiltonian can be transformed directly from Eq. (A3):

$$H(\mathbf{q},\mathbf{p}) = \sum_{i=1}^{N} \frac{(\mathbf{p}_i + m_i \mathbf{q}_i \cdot \nabla \mathbf{u}) \cdot (\mathbf{p}_i + m_i \mathbf{q}_i \cdot \nabla \mathbf{u})}{2m_i} + V(\mathbf{q}). \tag{A8}$$

Furthermore, the equations of motion, Eqs. (A1) and (A2), can be transformed as well:

$$\dot{\mathbf{q}}_i = \frac{\mathbf{p}_i}{m_i} + \mathbf{q}_i \cdot \nabla \mathbf{u}, \tag{A9}$$

$$\dot{\mathbf{p}}_i = \mathbf{F}_i - \mathbf{p}_i \cdot \nabla \mathbf{u} - m_i \mathbf{q}_i \cdot \nabla \mathbf{u} \cdot \nabla \mathbf{u}. \tag{A10}$$

These are the p-SLLOD equations of motion, and the Hamiltonian of Eq. (A8) is the conserved quantity in this algorithm,[10] i.e., $dH/dt=0$.

Although $H(\mathbf{q},\mathbf{p})$ as given by Eq. (A8) is still a conserved quantity in the frame of moving coordinates, it is no longer associated with the internal energy as calculated by an observer in this reference frame. According to the principle of frame indifference (also called the principle of material objectivity[21,22]), the internal energy and the pressure tensor in this reference frame have the same forms as in the laboratory reference frame:

$$H_0(\mathbf{q},\mathbf{p}) = \sum_{i=1}^{N} \frac{\mathbf{p}_i \cdot \mathbf{p}_i}{2m_i} + V(\mathbf{q}), \tag{A11}$$

$$\mathbf{P} = \left\langle \frac{1}{V} \sum_{i=1}^{N} \left(\frac{\mathbf{p}_i \mathbf{p}_i}{m_i} + \mathbf{q}_i \mathbf{F}_i \right) \right\rangle. \tag{A12}$$

Hence the rate of internal energy change in the moving coordinates no longer vanishes. However, since the moving reference frame is translating at constant velocity relative to the inertial laboratory frame, the moving framework must be inertial too; ergo, Newton's equation is also satisfied in the moving frame.

Keep in mind that $dH/dt=0$ is valid for a system seen from the point of view of the laboratory reference frame, which is the same point of view in which the p-SLLOD algorithm was developed.[10] In order to understand how the p-SLLOD algorithm behaves in the point of view of the standard NEMD reference frame (i.e., from the point of view in which the SLLOD algorithm was developed), it is necessary to examine this algorithm in that frame directly. This is the subject of Appendix B.

TABLE II. The same as in Table I, but using the p-SLLOD algorithm. Note that no phase transition occurs at low elongational rates, such as $\dot{\epsilon}=0.05$, 0.1, and 0.2.

$\dot{\epsilon}$	E_{int}/N	P_{xx}	P_{yy}	P_{zz}	η
0.05	1.812(0.041)	6.187(0.198)	6.644(0.215)	6.413(0.206)	2.288(1.292)
0.1	1.819(0.042)	6.023(0.193)	6.907(0.226)	6.446(0.207)	2.211(0.651)
0.2	1.839(0.042)	5.790(0.183)	7.438(0.248)	6.536(0.214)	2.060(0.338)
0.4	1.890(0.046)	5.504(0.180)	8.486(0.306)	6.744(0.231)	1.864(0.193)
0.5	1.921(0.049)	5.427(0.183)	9.022(0.337)	6.857(0.241)	1.797(0.165)
0.8	2.047(0.068)	5.428(0.212)	10.79(0.460)	7.339(0.309)	1.676(0.129)
1.0	2.168(0.086)	5.624(0.245)	12.19(0.536)	7.855(0.354)	1.641(0.119)
1.6	2.781(0.123)	7.080(0.322)	17.85(0.807)	10.53(0.473)	1.683(0.111)
2.0	3.429(0.152)	8.663(0.374)	22.96(1.050)	13.25(0.600)	1.787(0.113)
2.5	4.537(0.203)	11.27(0.471)	31.01(1.419)	17.61(0.809)	1.974(0.122)
3.2	6.777(0.292)	16.29(0.615)	46.21(2.102)	25.94(1.186)	2.338(0.140)

APPENDIX B: THERMODYNAMIC CONSISTENCY IN THE *p*-SLLOD ALGORITHM

In this appendix, we discuss one criterion of thermodynamic consistency of the *p*-SLLOD algorithm. Typically, it is expected that a NEMD algorithm should give rise to a time derivative of the internal energy in a macroscopic, adiabatic system possessing the functional form

$$\frac{dE_{\text{int}}}{dt} = -\mathbf{P}V_s:(\nabla \mathbf{u})^T. \tag{B1}$$

In Eq. (B1), V_s is the system volume and the other symbols are defined as in the main body of the paper. In this appendix, the *p*-SLLOD algorithm is viewed in the same conceptual sense as a typical NEMD simulation, i.e., it is viewed as representing an actual imposed flow field instead of the mathematical, virtual field of Appendix A. For arbitrary flow fields, an extra term can appear in the rate equation for the internal energy for *p*-SLLOD, which (as will be shown) is entirely consistent with the NEMD simulation concept.

In order to make this explanation as clear as possible, we first present two examples that illustrate that the definitions of thermodynamic and mechanical properties depend upon the point of view of the system under study. We then explore a precise connection between continuum and discrete mechanics. Finally, we apply our conclusions to the SLLOD and *p*-SLLOD algorithms.

First, we consider the phenomenon of particle disintegration in a laboratory frame of reference. Suppose that a mother particle, with mass M and velocity $\mathbf{u}$, becomes suddenly disintegrated into two daughter particles, with one particle having mass m_1 and velocity $\mathbf{u}_1$, and the other, mass m_2 and velocity $\mathbf{u}_2$. As is well known, there then exist seven integrals of motion: energy, three components of linear momentum, and three components of angular momentum:

$$E_{\text{int}} + K = (e_{\text{int }1} + k_1) + (e_{\text{int }2} + k_2), \tag{B2}$$

$$\mathbf{p} = \mathbf{p}_1 + \mathbf{p}_2, \tag{B3}$$

$$\mathbf{L} = \mathbf{l}_1 + \mathbf{l}_2. \tag{B4}$$

Here, E_{int}, K, $\mathbf{p}$, and $\mathbf{L}$ denote, respectively, the internal energy (i.e., the rest energy in a relativistic sense), kinetic energy of the center of mass of the system (COM kinetic energy), linear momentum, and angular momentum of the mother system. Correspondingly, the lowercase letters e_{int}, k, $\mathbf{p}$, and $\mathbf{l}$ denote the properties of a daughter system (subscripts 1 and 2 refer to each of the two daughter systems).

Let us consider more specifically the physical meaning of the internal energy. By accepted convention, the internal energy of a system does not contain the COM kinetic energy of the system. If we consider one of the daughter particles (say 1) as the physical system of interest, k_1 is regarded as the COM kinetic energy of system 1, and is therefore excluded from the internal energy. Now if we set up another big system enclosing the two subsystems by a hypothetical perfectly elastic wall with no mass, then the big system would be the original mother system with the same values of E_{int}, K, $\mathbf{p}$, and $\mathbf{L}$. In general, the COM velocity of the mother system is different than the COM velocity of either daughter system considered independently, and therefore the COM kinetic energy of the mother system is not equal to the sum of the kinetic energies of the two daughter systems. As a result, the internal energy of the mother system is not equal to the sum of the internal energies of the two daughter systems. This logical argument indicates that whenever we calculate the internal energy of a system, we should first calculate the velocity of the center of mass of the system, and then calculate the internal energy using each particle velocity relative to the velocity of the center of mass (COM velocity); this is the so-called ''peculiar velocity'' of the particle. This consideration applies equally to any physical system, whether the system is closed with a physical wall or open (as in continuum fluid mechanics, (i.e., hydrodynamics).

Next let us consider a more practical example. Suppose that there are two identical thermodynamic systems in equilibrium with no COM velocity. Suppose that we suddenly impose a COM velocity $+\mathbf{u}$ to one system and $-\mathbf{u}$ to the other without disrupting the internal state of either system (this can be done by using two moving frames of reference with velocities $\pm\mathbf{u}$). Then each system will have the same COM kinetic energy k in addition to its initial internal energy. We can then create a big system by enclosing the two systems within a perfectly elastic wall that has a volume equal to twice the original volume of each subsystem. Since the sum of the two subsystems' momenta is zero, the COM velocity of the big system is zero. After a certain time, the big system will reach a thermodynamic equilibrium. Now we ask the following questions: ''What is the temperature and pressure of the big system? Is it the same as that of the subsystems?'' Obviously, the answer is ''no,'' because the COM kinetic energies of the subsystems have been transformed into the kinetic part of the internal energy of the big system. In other words, the internal energy of the big system is composed not only of the sum of the internal energies of the two subsystems, but also of the sum of their COM kinetic energies as well.

These two examples show clearly that physical quantities depend on the definition of the system under consideration, as in Appendix A. In nonequilibrium physical processes with an external velocity field in space, regardless of whether or not the field is time dependent, we usually deal with an infinitesimal portion of fluid with a certain streaming velocity $\mathbf{u}$. The traditional conservation laws of mass, momentum, and energy are derived for the infinitesimal volume element (of course, the infinitesimal element is assumed to be of thermodynamic scale, i.e., composed of numerous particles). According to standard practice, the internal states of the system would not change at all for any inertial frame of reference moving with a constant velocity (we are here not concerned with any relativistic effect). Thus, we may set up a moving hypothetical boundary with the same velocity as that of the infinitesimal element of interest and employ the local equilibrium assumption to impart physical quantities defined by equilibrium thermodynamics such as temperature and pressure.

As before, let us consider a combined system of two identical infinitesimal systems of fluid, but with different streaming velocities (say, $\mathbf{u}_1$ and $\mathbf{u}_2$) in a nonequilibrium

process. As seen in the previous examples, physical quantities such as the internal energy per mass and the pressure tensor of the combined system, in general, would not be arithmetic averages of the two subsystems because the streaming velocity of the combined system, **u**, is not the same as either $\mathbf{u}_1$ or $\mathbf{u}_2$. Therefore, the peculiar velocity (or momentum) of particles needs to be recalculated relative to **u**. In other words, in the derivation of the traditional conservation equations, the same COM velocity is used as the reference velocity in the definition of the peculiar velocity, for all particles that exist within the differential element. However, in a NEMD simulation, the same COM velocity *is not used* to define the individual peculiar velocities; the individual peculiar velocities are defined with reference to the imposed velocity gradient This discrepancy introduces a fundamental difference between continuum theory and molecular-level simulation.

Such an inconsistency has frequently been adopted in NEMD simulations in connection with hydrodynamics. Specifically, the streaming velocity in field-driven NEMD simulations (DOLLS, SLLOD, and p-SLLOD) is different for different positions in the simulation box according to the imposed velocity gradient field $\nabla\mathbf{u}$. Furthermore, the COM velocity used in the definition of the peculiar velocities of the particles is thus different for the various particles. Nevertheless, the internal energy and pressure tensor have been calculated over all particles in the box. Although such expressions have their own physical meanings, they are not precisely consistent with hydrodynamics. In some special cases, such as that of a constant pressure tensor throughout space (e.g., planar Couette flow and PEF), the pressure tensor expression over all the particles in a simulation may be regarded as an average over space. However, in the case of position-dependent pressure tensor (e.g., Hagen-Poiseuille flow), such an expression would not be the appropriate one.

Now let us consider three conservation laws of mass, linear momentum, and energy for an infinitesimal fluid region moving with a streaming velocity **u**:

$$\frac{D\rho}{Dt} = -\rho\nabla\cdot\mathbf{u}, \tag{B5}$$

$$\rho\frac{D\mathbf{u}}{Dt} = -\nabla\cdot\mathbf{P}, \tag{B6}$$

$$\rho\frac{D\hat{E}_{\mathrm{int}}}{Dt} = -\nabla\cdot\mathbf{J}_q - \mathbf{P}:(\nabla\mathbf{u})^T. \tag{B7}$$

Note that the time derivatives on the left-hand side of these expressions are the material or substantial derivatives. Here, ρ is the mass density, $\hat{E}_{\mathrm{int}}$ is the internal energy per unit mass, $\mathbf{J}_q$ is the heat flux, and **P** is the pressure tensor. E_{int} and **P** in terms of particle coordinates (position and velocity) are written as

$$E_{\mathrm{int}} = \sum_{i=1}^{n_R} \frac{1}{2} m_i(\mathbf{v}_i' - \mathbf{u})^2 + V(\mathbf{q}), \tag{B8}$$

$$\mathbf{P}v = \sum_{i=1}^{n_R} [m_i\mathbf{v}_i'(\mathbf{v}_i' - \mathbf{u}) + \mathbf{q}_i\mathbf{F}_i], \tag{B9}$$

where v is the volume of the infinitesimal portion and n_R is the number of particles in this volume. $\mathbf{v}_i'$ and $\mathbf{q}_i$ are the laboratory velocity and position vector of particle i, respectively, $V(\mathbf{q})$ is the potential energy, and $\mathbf{F}_i$ is the force acting on particle i. Note that only the particles in the infinitesimal portion under consideration are to be included in the summation. The first term on the RHS of Eq. (B9), representing the kinetic part of the pressure tensor, has the physical meaning that particles with nonzero velocities relative to the streaming velocity **u** of the infinitesimal region under consideration would make a contribution of their momentum to the pressure tensor; therefore, they would also contribute to the total momentum of the infinitesimal region. Denoting the peculiar velocity of particle i as $\mathbf{v}_i(=\mathbf{v}_i' - \mathbf{u})$, Eq. (B9) can be rewritten as

$$\begin{aligned}\mathbf{P}v &= \sum_{i=1}^{n_R} m_i(\mathbf{v}_i + \mathbf{u})\mathbf{v}_i + \mathbf{q}_i\mathbf{F}_i \\ &= \sum_{i=1}^{n_R} (m_i\mathbf{v}_i\mathbf{v}_i + \mathbf{q}_i\mathbf{F}_i) + \sum_{i=1}^{n_R} \mathbf{u}m_i\mathbf{v}_i.\end{aligned} \tag{B10}$$

The last term on the RHS of Eq. (B10) is necessarily zero from the definition of the peculiar and streaming velocities, $\mathbf{u}(=\Sigma_i m_i\mathbf{v}_i'/\Sigma_i m_i)$. Thus, the resulting expression has the conventional form of the pressure tensor in hydrodyamics. In NEMD simulations using field-driven NEMD algorithms, **u** is not calculated from the particle velocity within each small region in the simulation box. Instead, it is included as a known parameter in the equations of motion in the form of $\nabla\mathbf{u}$.

Now let us consider the expression for the internal energy in the SLLOD and p-SLLOD algorithms. Consistently with hydrodynamics, we should consider only a small region of the total simulation volume. It is essential to realize that the total simulation volume must be treated as larger than this small element of volume because the streaming velocity **u** varies within the simulation volume, but cannot vary within the small element. The internal energy and its time derivative are given by

$$E_{\mathrm{int}} = \sum_{i=1}^{n_R} \frac{\mathbf{p}_i^2}{2m_i} + V(\mathbf{q}), \tag{B11}$$

$$\frac{dE_{\mathrm{int}}}{dt} = \sum_{i=1}^{n_R} \frac{\dot{\mathbf{p}}_i\cdot\mathbf{p}_i}{m_i} - \dot{\mathbf{q}}_i\cdot\mathbf{F}_i. \tag{B12}$$

Using the equations of motion of the DOLLS, SLLOD, and p-SLLOD algorithms, the expressions for dE_{int}/dt are found to be

DOLLS and SLLOD

$$\frac{dE_{\text{int}}}{dt} = -\sum_{i=1}^{n_R} \left(\frac{\mathbf{p}_i \mathbf{p}_i}{m_i} + \mathbf{q}_i \mathbf{F}_i \right) : (\boldsymbol{\nabla} \mathbf{u})^T = -\mathbf{P} v : (\boldsymbol{\nabla} \mathbf{u})^T, \tag{B13}$$

p-SLLOD

$$\begin{aligned} \frac{dE_{\text{int}}}{dt} &= -\sum_{i=1}^{n_R} \left(\frac{\mathbf{p}_i \mathbf{p}_i}{m_i} + \mathbf{q}_i \mathbf{F}_i + (\mathbf{q}_i \cdot \boldsymbol{\nabla} \mathbf{u}) p_i \right) : (\boldsymbol{\nabla} \mathbf{u})^T \\ &= -\tilde{\mathbf{P}} v : (\boldsymbol{\nabla} \mathbf{u})^T, \end{aligned} \tag{B14}$$

where $\tilde{\mathbf{P}}$ denotes the quantity with the parentheses in Eq. (B14). Note that Eq. (B14) may be rewritten as

$$\frac{dE_{\text{int}}}{dt} = -\sum_{i=1}^{n_R} \left(\frac{\mathbf{p}_i (\mathbf{p}_i + m_i \mathbf{q}_i \cdot \boldsymbol{\nabla} \mathbf{u})}{m_i} + \mathbf{q}_i \mathbf{F}_i \right) : (\boldsymbol{\nabla} \mathbf{u})^T. \tag{B15}$$

Hence we recognize the analogy between (i) the quantity in the large parentheses and (ii) the first line of equality in Eq. (B10). In all field-driven NEMD algorithms, we set $\mathbf{u}_i = \mathbf{q}_i \cdot \boldsymbol{\nabla} \mathbf{u}$ for each particle. As mentioned above, $\mathbf{P}$ and $\tilde{\mathbf{P}}$ are exactly the same in hydrodynamics since $\mathbf{u}_i = \mathbf{q}_i \cdot \boldsymbol{\nabla} \mathbf{u} = \mathbf{u} = \mathbf{q} \cdot \boldsymbol{\nabla} \mathbf{u}$, where $\mathbf{q}$ (in the range of $\mathbf{q}$ to $\mathbf{q} + d\mathbf{q}$) represents the position vector of the infinitesimal region in space. The sum of the $\mathbf{p}_i$ is identically zero by definition. Although the extra term in the internal energy derivative of Eq. (B15) can be finite in simulations, at the continuum level this term vanishes.

Therefore, we see that the p-SLLOD algorithm satisfies not only Newtonian mechanics as shown in the main body of the paper, but also the thermodynamic criterion, (i.e., it produces the correct macroscopic equation of change for the internal energy), whereas the SLLOD algorithm satisfies thermodynamics, but not Newtonian mechanics.

[1] W. G. Hoover, D. J. Evans, R. B. Hickman, A. J. C. Ladd, W. T. Ashurst, and B. Moran, Phys. Rev. A **22**, 1690 (1980).
[2] D. J. Evans and G. P. Morriss, Phys. Rev. A **30**, 1528 (1984).
[3] D. J. Evans and G. P. Morriss, *Statistical Mechanics of Nonequilibrium Liquids* (Academic, New York, 1990).
[4] B. D. Todd and P. J. Daivis, Phys. Rev. Lett. **81**, 1118 (1998).
[5] A. M. Kraynik and D. A. Reinelt, Int. J. Multiphase Flow **18**, 1045 (1992).
[6] A. Baranyai and P. T. Cummings, J. Chem. Phys. **110**, 42 (1999).
[7] B. D. Todd and P. J. Daivis, Comput. Phys. Commun. **117**, 191 (1999).
[8] B. D. Todd and P. J. Daivis, J. Chem. Phys. **112**, 40 (2000).
[9] M. E. Tuckerman, C. J. Mundy, S. Balasubramanian, and M. L. Klein, J. Chem. Phys. **106**, 5615 (1997).
[10] B. J. Edwards and M. Dressler, J. Non-Newtonian Fluid Mech. **96**, 163 (2001).
[11] H. Goldstein, *Classical Mechanics*, 2nd Ed. (Addison-Wesley, Reacling, MA, 1980).
[12] A. W. Lees and S. F. Edwards, J. Phys. C **5**, 1921 (1972).
[13] S. Nosé, Mol. Phys. **52**, 255 (1984).
[14] S. Nosé, J. Chem. Phys. **81**, 511 (1984).
[15] W. G. Hoover, Phys. Rev. A **31**, 1695 (1985).
[16] J. Delhommelle and D. J. Evans, J. Chem. Phys. **115**, 43 (2001).
[17] L. Lue, O. G. Jepps, J. Delhommelle, and D. J. Evans, Mol. Phys. **100**, 2387 (2002).
[18] C. J. Mundy, J. I. Siepmann, and M. L. Klein, J. Chem. Phys. **103**, 10192 (1995).
[19] J. D. Weeks, D. Chandler, and H. C. Andersen, J. Chem. Phys. **54**, 5237 (1971).
[20] M. P. Allen and D. J. Tildesley, *Computer Simulation of Liquids* (Clarendon, Oxford, 1987).
[21] C. Truesdell, Meccanica **11**, 196 (1976).
[22] C. Truesdell, *Rational Thermodynamics*, 2nd ed. (Springer, New York, 1984).